

PAPER

Distinct behavior of electronic structure under uniaxial strain in BaFe_2As_2

To cite this article: Jiajun Li *et al* 2023 *Chinese Phys. B* **33** 017401

View the [article online](#) for updates and enhancements.

You may also like

- [The growth of 122 and 11 iron-based superconductor single crystals and the influence of doping](#)
D P Chen and C T Lin
- [Pressure-induced electronic phase transition and superconductivity in spin-ladder compounds \$\text{BaFe}_2\(\text{S}_{1-x}\text{Se}_x\)_2\$](#)
Y J Fan, J Y Liu, J J Feng *et al.*
- [High-pressure polymorphism of \$\text{BaFe}_2\text{Se}_3\$](#)
V Svitlyk, G Garbarino, A D Rosa *et al.*

Distinct behavior of electronic structure under uniaxial strain in BaFe₂As₂

Jiajun Li(李佳俊)^{1,2,†}, Giao Ngoc Phan^{1,3,†}, Xingyu Wang(王兴玉)^{1,2,†}, Fazhi Yang(杨发枝)^{1,2}, Quanxin Hu(胡全欣)^{1,2}, Ke Jia(贾可)^{1,2,4}, Jin Zhao(赵金)^{1,2}, Wenyao Liu(刘文尧)^{1,2}, Renjie Zhang(张任杰)^{1,2}, Youguo Shi(石友国)^{1,2,4,5}, Shiliang Li(李世亮)^{1,2,5}, Tian Qian(钱天)^{1,5}, and Hong Ding(丁洪)^{1,3,6,‡}

¹Beijing National Laboratory for Condensed Matter Physics and Institute of Physics, Chinese Academy of Sciences, Beijing 100190, China

²School of Physics, University of Chinese Academy of Sciences, Beijing 100190, China

³CAS Center for Excellence in Topological Quantum Computation, University of Chinese Academy of Sciences, Beijing 100190, China

⁴Center of Materials Science and Optoelectronics Engineering, University of Chinese Academy of Sciences, Beijing 100049, China

⁵Songshan Lake Materials Laboratory, Dongguan 523808, China

⁶Tsung-Dao Lee Institute, Shanghai Jiao Tong University, Shanghai 201210, China

(Received 6 April 2023; revised manuscript received 24 May 2023; accepted manuscript online 25 May 2023)

We report a study of the electronic structure of BaFe₂As₂ under uniaxial strains using angle-resolved photoemission spectroscopy and transport measurements. Two electron bands at the M_Y point, with an energy splitting of 50 meV in the strain-free sample, shift downward and merge into each other under a large uniaxial strain, while three hole bands at the Γ point shift downward together. However, we also observed an enhancement of the resistance anisotropy under uniaxial strains by electrical transport measurements, implying that the applied strains strengthen the electronic nematic order in BaFe₂As₂. These observations suggest that the splitting of these two electron bands at the M_Y point is not caused by the nematic order in BaFe₂As₂.

Keywords: iron-based superconductor, angle-resolved photoelectron spectroscopy, uniaxial strain, symmetry breaking

PACS: 74.25.Jb, 74.25.F–

DOI: 10.1088/1674-1056/acd8af

1. Introduction

BaFe₂As₂, well known for its rich phase diagram and interplay among various orders, provides a good material system for studying many novel properties, such as the superconducting mechanism of iron-based superconductors.^[1–7] In BaFe₂As₂, as the temperature decreases, the sample undergoes an antiferromagnetic phase transition as well as a structural phase transition.^[8,9] With the structural phase transition, the sample changes from an original single-domain state to two orthogonal twinned crystal phase compositions and exhibits a new electronic nematic order near the phase transition temperature, which has been observed in previous studies on iron-based superconductors by a scanning tunneling microscope (STM) and angle-resolved photoemission spectroscopy (ARPES) at low temperatures.^[10–13] Considering the simultaneous appearance of nematic order, antiferromagnetic order and superconductivity, it is challenging to independently study these strongly correlated intertwined properties. Therefore, finding a method to independently study the nature of the nematic order without introducing the influence of other orders is highly desirable. In previous studies, a single domain state has been obtained in detwinned BaFe₂As₂ by applying a small uniaxial strain wherein an electronic nematic order was observed.^[14–16] By further applying a considerable uniaxial

strain to BaFe₂As₂, the in-plane anisotropy of the resistance, which is closely related to the nematic order, would be further enhanced.^[17,18] On the other hand, while a study on FeSe has revealed that the band positions corresponding to different electric orbitals shift differently under a larger strain,^[19] it is still worth studying how band positions shift when a larger uniaxial strain is applied to BaFe₂As₂.

In this paper, we present the evolution of the electronic properties of BaFe₂As₂ under uniaxial strains. The observed transport results demonstrate that uniaxial strains can enhance the nematic order. On the other hand, at the M_Y point, the upper electron band is drastically shifted toward the lower one. Consequently, the energy splitting between these two electron bands diminishes under a large uniaxial strain, even though the nematic order is enhanced. These surprising behaviors suggest that the band splitting at the M_Y point is not induced by the nematic order in BaFe₂As₂.

2. Methods

Single crystals of BaFe₂As₂ were grown by a self-flux method. The samples with better single-crystal quality were selected, which could withstand larger strains and show clearer band dispersions. Considering that a strain would be applied along the [1 1 0] direction in the ab plane, crystal structure of

[†]These authors contributed equally to this work.

[‡]Corresponding author. E-mail: dingh@sjtu.edu.cn

BaFe₂As₂ in the *ab* plane is shown in Fig. 1(a). The upper inset in Fig. 1(a) shows the strain device, which can continuously apply uniaxial strains to the mounted sample by turning the screw. With this design, an *in situ* strain along one desirable direction can be applied to the sample. Here, we use the Brillouin zone (BZ) notations corresponding to the true crystallographic unit cell of two Fe atoms, in which Γ - M_Y is along the [1 1 0] direction and Γ - M_X is along the [1 -1 0] direction, as shown in Fig. 1(b).

High-resolution ARPES measurements were carried out at the Institute of Physics, Chinese Academy of Sciences, with an R4000 analyzer with a He discharge lamp ($h\nu = 21.2$ eV). The angular and momentum resolutions were set to 0.2° and 4 meV, respectively. To clearly study the electron band characteristics at the boundary of the BaFe₂As₂ Brillouin zone, the direction of applied strain was set to be perpendicular to the electron-receiving slit of the ARPES analyzer, as shown in Fig. 1(c). In order to keep the same cleave surfaces, all samples in this paper were cleaved *in situ* at room temperature in a chamber with a vacuum of 1×10^{-10} Torr, and As dimer surfaces were obtained.^[20–22] For all of the ARPES measurements described below, the temperature is 14 K and the vacuum is better than 3×10^{-11} Torr.

The in-plane uniaxial strains were applied to a single crystal of BaFe₂As₂ by turning the screw of a strain device on which the sample is mounted, and thus the screw move-

ments could be deemed to be the deformations δL of the sample in the direction of applied strains.^[23] The uniaxial strain strength $\delta L/L$ is defined as the ratio of the screw movement to the original length L of the sample, which was measured directly before mounting it.

The changes in lattice constants indicated by XRD results prove that it is reliable to regard the screw movements as the deformations of the sample. The specific calculation method is as follows. Considering that the lattice constant along the [2 2 0] direction of the sample cannot be directly measured by XRD due to the sample holder, we indirectly calculated the deformation and lattice constant along the [2 2 0] direction by measuring the lattice constants along the [0 0 12] and [2 2 12] directions. Figures 1(d) and 1(e) show the corresponding XRD results.

It is known that the interplanar spacing for the strain-free sample, denoted by d , is 1.08618 Å along the [0 0 12] direction and 0.8573 Å along the [2 2 12] direction. Strains S1, S2, S3 and S4, which represent four gradually increasing uniaxial strains, were applied to the samples in turn. Taking strain S1 as an example, by substituting diffraction angles θ before and after applying uniaxial strain into the Bragg diffraction formula, $2d \times \sin(\theta) = n\lambda$, the interplanar spacing for the strained sample, denoted by d_{S1} , is 1.08497 Å along the [0 0 12] direction and 0.8551 Å along the [2 2 12] direction.

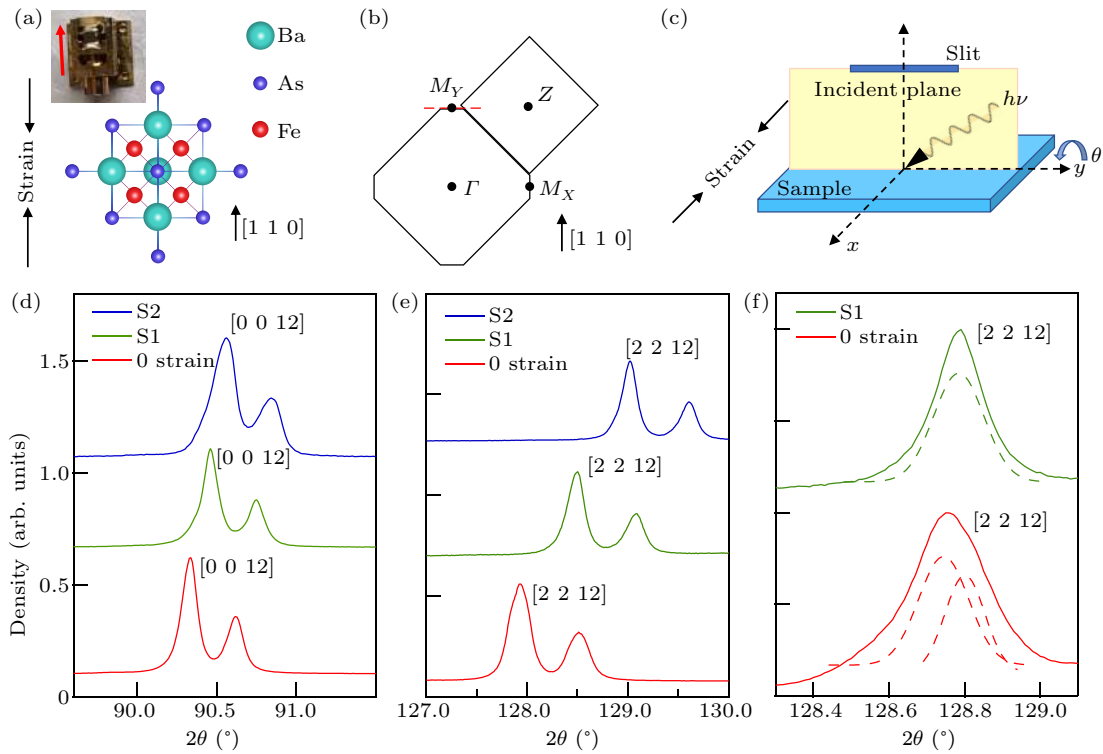


Fig. 1. (a) Crystal structure of BaFe₂As₂ in the *ab* plane with a uniaxial strain applied along the [1 1 0] direction. Upper inset: picture of the *in situ* strain device (with sample). A red arrow indicates the direction in which strain is applied. Strain can be sequentially enhanced by turning the screw. (b) Schematic of the corresponding in-plane Brillouin zone for two Fe atoms per unit cell. (c) Schematic of the ARPES experiment. The direction of applied strain is perpendicular to the electron-receiving slit of the ARPES analyzer. [(d), (e)] XRD results at room temperature for (d) [0 0 12] and (e) [2 2 12] Bragg peaks under different applied strains of 0, S1 and S2 at room temperature. Shifts of the Bragg peak indicate the changes in lattice constants. (f) XRD results at 90 K for the sample under zero strain and under the minimum uniaxial strain S1.

According to the formula

$$\left(\frac{1}{d_{[hkl]}}\right)^2 = \left(\frac{h}{a}\right)^2 + \left(\frac{k}{b}\right)^2 + \left(\frac{l}{c}\right)^2, \quad (1)$$

where h , k and l denote Miller indices, c_{S1} for the $[0\ 0\ 1]$ direction is derived as $13.0196\ \text{\AA}$ when $d_{S1[0012]}$ is $1.08497\ \text{\AA}$, and then a_{S1} for the $[1\ 1\ 0]$ direction is derived as $5.5574\ \text{\AA}$. Thus, the change in lattice constant $(a_{S1} - a)/a$ is -0.49% . On the other hand, for strain S1, the screw movement is $0.0175\ \text{mm}$, the original length L of the sample is $3.5\ \text{mm}$ and the ratio of the two is 0.5% , which is consistent with $(a_{S1} - a)/a_0$ of -0.49% calculated from the XRD results.

Similarly, for strain S2, $(a_{S2} - a)/a$ calculated from the XRD results is -0.84% . The screw movement for strain S2 is $0.025\ \text{mm}$, the original length L of the sample is $2.8\ \text{mm}$ and the ratio of the two is 0.89% , which is consistent with $(a_{S2} - a)/a$ of -0.84% .

Therefore, it is reliable to define uniaxial strain strength $\delta L/L$ as the ratio of screw movement to the original length of the sample at room temperature. For cases at low temperature we take the thermal expansion coefficients into account, which are 17.0×10^{-6} for BeCu (C17200) in the strain device and 18.9×10^{-6} for BaFe_2As_2 ; we found the difference

caused by thermal expansion coefficients is 0.995 at $14\ \text{K}$. Thus, $\delta L/L$ at $14\ \text{K}$ is -0.498% under strain S1 and -0.889% under strain S2. By the same method, strain strengths $\delta L/L$ corresponding to strains S3 and S4 can be obtained as 1.357% and 2.001% , respectively.

XRD at a low temperature of $90\ \text{K}$, for both the strain-free sample and the S1 strained sample, was measured as shown in Fig. 1(f). It can be clearly observed that under zero strain, the $[2\ 2\ 12]$ Bragg peak splits due to the twinning effect at low temperatures, showing two structural domains in a strain-free sample. For the S1 strained sample, there is only one $[2\ 2\ 12]$ Bragg peak at low temperature, indicating that the sample remains in a single-domain state under the minimum uniaxial strain S1. It is worth mentioning that the strains in this report are much stronger than those in previous reports for detwinned samples that exhibit nematic order.^[24]

With increasing strains, the in-plane transport anisotropy of BaFe_2As_2 becomes stronger, as shown in Fig. 2, which implies a stronger nematic order in strained BaFe_2As_2 , in good agreement with previous reports.^[17,18] In Fig. 2, R_b and R_a correspond to the resistances measured along the $[1\ 1\ 0]$ direction and the $[1\ -1\ 0]$ direction respectively on the same samples and normalized by the resistances at $300\ \text{K}$.

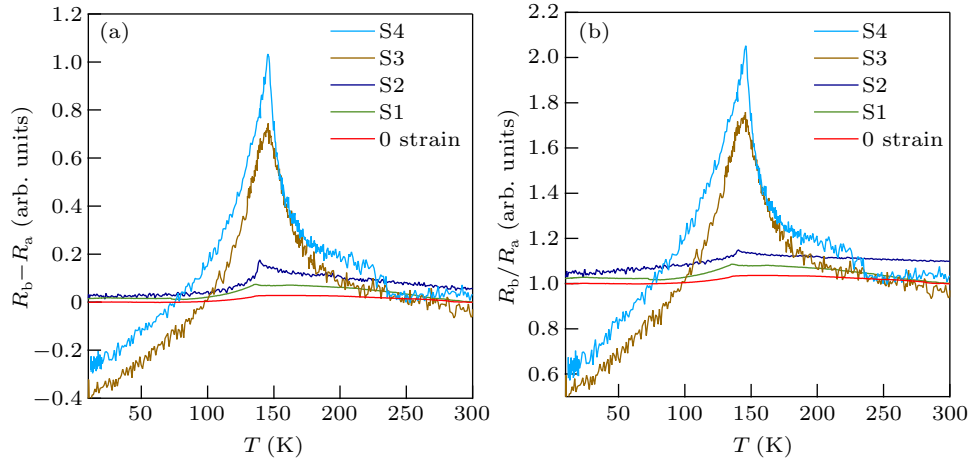


Fig. 2. The in-plane resistance anisotropy indicated by (a) $R_b - R_a$ and (b) R_b/R_a for five typical strained samples. The more heavily strained samples S4 and S3 exhibit stronger anisotropy than the moderately strained samples S2 and S1.

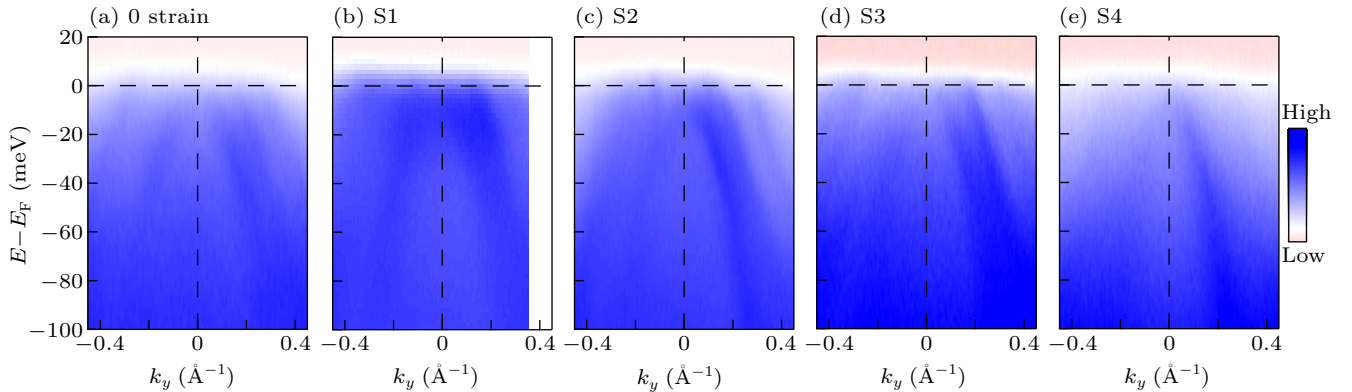


Fig. 3. ARPES intensity plots measured around the Γ point for (a) strain-free and (b)–(e) increasingly strained BaFe_2As_2 samples. S1, S2, S3 and S4 represent four gradually increasing uniaxial strains. The three hole bands shift downward under the increasing uniaxial strains.

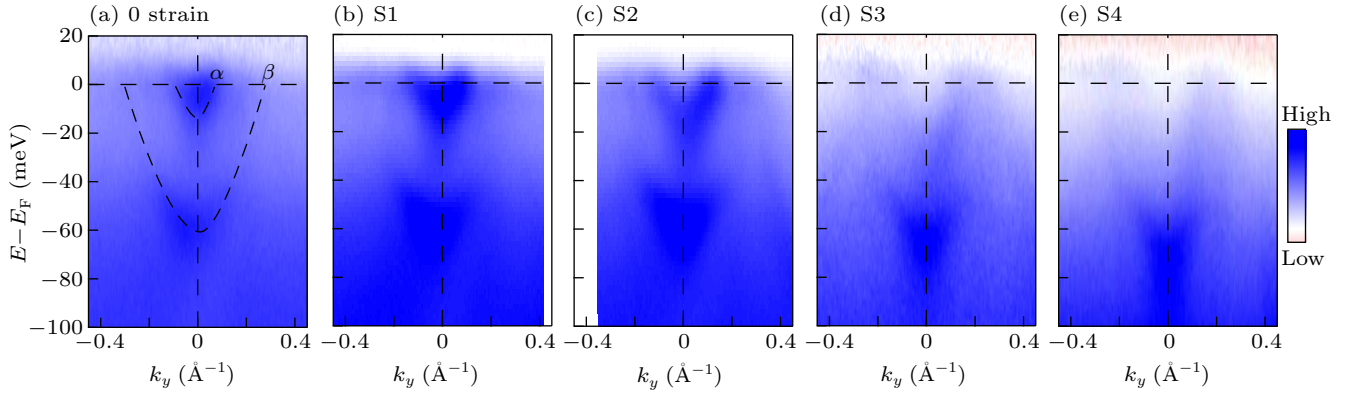


Fig. 4. ARPES intensity plots measured around the M_Y point for (a) strain-free and (b)–(e) increasingly strained BaFe_2As_2 samples. The two electron bands shift downward under the increasing uniaxial strains. The upper electron band (α band) is more sensitive to the strains, while the lower one (β band) shifts slightly under the applied strains. The black dashed lines are guides for the eyes.

3. Experimental results

Figure 3 shows the evolution of electronic structure with increasing uniaxial strains around the Γ point. A strain-free sample exhibits three hole bands near the Fermi level similar to previous reports.^[15,25] With increasing uniaxial strains, the three hole bands shift downward by less than 13 meV, similar to the previous report on the variation of hole bands near the Γ point under uniaxial strains in iron-based superconductors.^[19] It is well known that the splitting of hole bands at the Γ point is independent of the nematic order.^[13] Therefore, the downward shifts of the three hole bands here can be considered to be a result of lattice distortions caused by the uniaxial strains.

Figure 4 shows the evolution of electronic structure with increasing uniaxial strains around the M_Y point. A strain-free sample exhibits two electron bands near the Fermi level, similar to previous reports.^[15,25] With increasing uniaxial strains, the electron bands shift downward at different rates. The upper electron band (α band) shifts downward significantly while the lower one (β band) shifts slightly. As a result, the upper band shifts toward the lower one, and eventually these two bands merge into each other at the M_Y point.

In previous studies of the detwinned sample under a smaller uniaxial strain, it was reported that the positions of the bottoms of the two electron bands at the M_Y point do not shift significantly before or after the detwinning.^[14,15] However, in this paper, when a larger strain is applied to the sample, it is directly observed from the spectra that the bottoms of two electron bands gradually merge under the increasing uniaxial strains. Moreover, the transport results in Fig. 2 imply that a larger uniaxial strain leads to a stronger nematic order. That is, with the increasing strains, the splitting of two electron bands decreases although the nematic order becomes stronger. Therefore, it can be concluded that the splitting of these two electron bands is not induced by the nematic order.

In order to quantitatively analyze the effect of strains at the M_Y point, we extract the energy distribution curves (EDCs) and energy positions of the bottoms of the two electron bands

under different strains, as shown in Figs. 5(a) and 5(b), respectively. As the uniaxial strain increases from S1 to S4, the bottom of the β band shifts from -60 meV to -72 meV, which is consistent with the trend at the Γ point as shown in Figs. 3(a)–3(e). However, the energy position of the bottom of the α band shows a different shift when the uniaxial strain is applied to the sample. It gradually shifts from -10 meV to -33 meV — a change of 23 meV — when the uniaxial strain increases from S1 to S3. Finally, under the uniaxial strain of S4, the bottom of the α band merges with the bottom of the β band. It can be seen that α band exhibits significantly more sensitivity to strain.

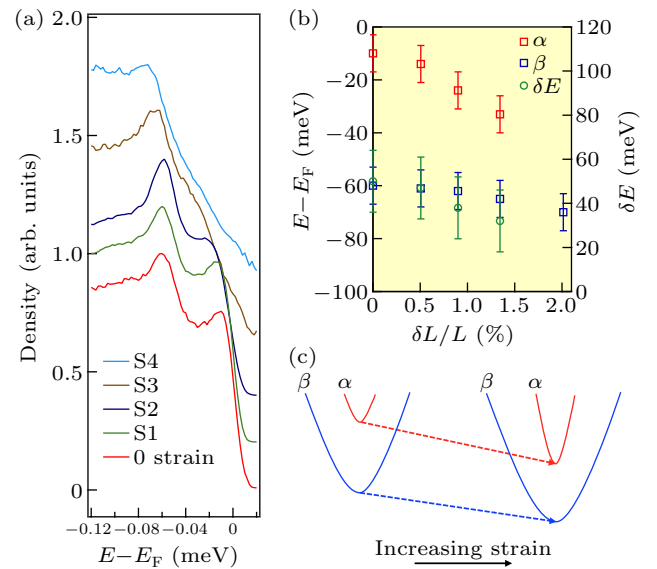


Fig. 5. (a) Comparison of EDCs extracted from Figs. 4(a)–4(e). Different colored lines indicate different applied strains of 0, S1, S2, S3 and S4, as shown in the diagram. (b) The energy positions of the bottoms of the α band and the β band and the energy distance δE between two bottoms of the electron band are plotted as functions of strain strength defined as the ratio between the deformation and the sample's size $\delta L/L$ in BaFe_2As_2 . (c) Schematic of the band structure at the M_Y point in BaFe_2As_2 . Also depicted is a diagram of the evolution in the two electron bands as the strain increases.

The difference between the bottoms of the two electron bands and their energy distance δE are also extracted in

Fig. 5(b). When no strain was applied to the sample, the energy distance δE between the two bottoms of the two electron bands was about 50 meV. When the strain is large enough, δE gradually decreases with increasing strains. This also proves that the two electron bands do not change uniformly under increasing strains.

4. Conclusion and perspectives

In previous studies of uniaxial strains in the BaFe_2As_2 system, it was found that the energy positions of different bands along two in-plane directions before and after detwinning changed only modestly. In this paper, varying uniaxial strains were applied to BaFe_2As_2 samples. Under increasing strains, three hole bands at the Γ point show similar shifts, which are affected by the lattice distortions. However, two electron bands at the M_Y point exhibit different properties: the shift of the β band is similar to that of the three hole bands at the Γ point. In contrast, a more significant shift of the α band is observed. Under a large strain, the two electron bands tend to close together even though the nematic order is enhanced. This clearly suggests that the splitting of these two electron bands is not induced by the nematic order.

Acknowledgments

Project supported by the National Natural Science Foundation of China (Grant Nos. 11888101 and U1832202), the Chinese Academy of Sciences (Grant Nos. QYZDB-SSW-SLH043, XDB28000000, and XDB33000000), the K. C. Wong Education Foundation (Grant No. GJTD-2018-01), and the Informatization Plan of Chinese Academy of Sciences (Grant No. CAS-WX2021SF-0102).

References

- [1] Chen G F, Li Z, Dong J, Li G, Hu W Z, Zhang X D, Song X H, Zheng P, Wang N L and Luo J L 2008 *Phys. Rev. B* **78** 224512
- [2] Rotter M, Tegel M and Johrendt D 2008 *Phys. Rev. Lett.* **101** 107006
- [3] Kimber S A J, Kreyssig A, Zhang Y Z, Jeschke H O, Valentí R, Yokaichiya F, Colombier E, Yan J Q, Hansen T C, Chatterji T, McQueeney R J, Canfield P C, Goldman A I and Argyriou D N 2009 *Nat. Mater.* **8** 471
- [4] Torikachvili M S, Bud'ko S L, Ni N and Canfield P C 2008 *Phys. Rev. B* **78** 104527
- [5] Ding H, Richard P, Nakayama K, Sugawara K, Arakane T, Sekiba Y, Takayama A, Souma S, Sato T, Takahashi T, Wang Z, Dai X, Fang Z, Chen G F, Luo J L and Wang N L 2008 *Europhys. Lett.* **83** 47001
- [6] Richard P, Sato T, Nakayama K, Souma S, Takahashi T, Xu Y M, Chen G F, Luo J L, Wang N L and Ding H 2009 *Phys. Rev. Lett.* **102** 047003
- [7] Christianson A D, Goremychkin E A, Osborn R, Rosenkranz S, Lumsden M D, Malliakas C D, Todorov I S, Claus H, Chung D Y, Kanatzidis M G, Bewley R I and Guidi T 2008 *Nature* **456** 930
- [8] Rotter M, Tegel M, Johrendt D, Schellenberg I, Hermes W and Pöttgen R 2008 *Phys. Rev. B* **78** 020503
- [9] Ni N, Bud'ko S L, Kreyssig A, Nandi S, Rustan G E, Goldman A I, Gupta S, Corbett J D, Kracher A and Canfield P C 2008 *Phys. Rev. B* **78** 014507
- [10] Rosenthal E P, Andrade E F, Arguello C J, Fernandes R M, Xing L Y, Wang X C, Jin C Q, Millis A J and Pasupathy A N 2014 *Nat. Phys.* **10** 225
- [11] Shimojima T, Suzuki Y, Sonobe T, Nakamura A, Sakano M, Omachi J, Yoshioka K, Kuwata-Gonokami M, Ono K, Kumigashira H, Böhmer A E, Hardy F, Wolf T, Meingast C, Löhneysen H V, Ikeda H and Ishizaka K 2014 *Phys. Rev. B* **90** 121111
- [12] Watson M D, Kim T K, Haghghirad A A, Davies N R, McCollam A, Narayanan A, Blake S F, Chen Y L, Ghannadzadeh S, Schofield A J, Hoesch M, Meingast C, Wolf T and Coldea A I 2015 *Phys. Rev. B* **91** 155106
- [13] Zhang P, Qian T, Richard P, Wang X P, Miao H, Lv B Q, Fu B B, Wolf T, Meingast C, Wu X X, Wang Z Q, Hu J P and Ding H 2015 *Phys. Rev. B* **91** 214503
- [14] Yi M, Lu D H, Chu J H, Analytis J G, Sorini A P, Kemper A F, Moritz B, Mod S K, Moore R G, Hashimoto M, Lee W S, Hussain Z, Devereaux T P, Fisher I R and Shen Z X 2011 *Proc. Natl. Acad. Sci. USA* **108** 6878
- [15] Pfau H, Rotundu C R, Palmstrom J C, Chen S D, Hashimoto M, Lu D H, Kemper A F, Fisher I R and Shen Z X 2019 *Phys. Rev. B* **99** 035118
- [16] Watson M D, Dudin P, Rhodes L C, Evtushinsky D V, Iwasawa H, Aswartham S, Wurmehl S, Büchner B, Hoesch M and Kim T K 2019 *npi Quantum Mater.* **4** 36
- [17] Malinowski P, Jiang Q N, Sanchez J J, Mutch J, Liu Z Y, Went P, Liu J, Ryan P J, Kim J W and Chu J H 2020 *Nat. Phys.* **16** 1189
- [18] Sanchez J J, Malinowski P, Mutch J, Liu J, Kim J W, Ryan P J and Chu J H 2021 *Nat. Mater.* **20** 1519
- [19] Phan G N, Nakayama K, Sugawara K, Sato T, Urata T, Tanabe Y, Tanigaki K, Nabeshima F, Imai Y, Maeda A and Takahashi T 2017 *Phys. Rev. B* **95** 224507
- [20] Masee F, Jong S D, Huang Y, Kaas J, Heumen E V, Goedkoop J B and Golden M S 2009 *Phys. Rev. B* **80** 140507
- [21] Jensen F M, Brouet V, Papalazarou E, Nicolaou A, Taleb-Ibrahimi A, Fèvre P L, Bertran F, Forget A and Colson D 2011 *Phys. Rev. B* **84** 014509
- [22] Hu Q X, Yang F Z, Wang X Y, Li J J, Liu W Y, Kong L Y, Li S L, Yan L, Xu J P and Ding H 2023 *Phys. Rev. Mater.* **7** 034801
- [23] Liu W Y, Hu Q X, Wang X C, Zhong Y G, Yang F Z, Kong L Y, Cao L, Li G, Peng Y, Okazaki K, Kondo T, Jin C Q, Xu J P, Gao H J and Ding H 2022 *Quantum Frontiers* **1** 20
- [24] He M Q, Wang L R, Ahn F, Hardy F, Wolf T, Adelman P, Schmalian J, Eremin I and Meingast C 2017 *Nat. Commun.* **8** 504
- [25] Yang X L, Zhang Y, Ou H W, Zhao F J, Shen D W, Zhou B, Wei J, Chen F, Xu M, He C, Chen Y, Wang Z D, Wang X F, Wu T, Wu G, Chen X H, Arita M, Shimada K, Taniguchi M, Lu Z Y, Xiang T and Feng D L 2009 *Phys. Rev. Lett.* **102** 107002